Test results of boron carbide ceramics for ITER port protection

Andrey Shoshin [a,b,]*, Alexander Burdakov [a,c], Maxim Ivantsivskiy [a], Sergey Polosatkin [a,b,c], Alexey Semenov [a,c], Yuliy Sulyaev [a,b], Evgenii Zaitsev [a], Polina Polozova [b], Sergey Taskaev [a,b], Dmitrii Kasatov [a,b], Ivan Shchudlo [a,b], Marina Bikchurina [b]

[a] Budker Institute of Nuclear Physic SB RAS, Novosibirsk, 630090, Russia
[b] Novosibirsk State University, Novosibirsk, 630090, Russia
[c] Novosibirsk State Technical University, Novosibirsk, 630092, Russia

ARTICLE INFO

ABSTRACT

The results of long-term outgassing test of large quantities of ceramics, which is planned to be used in ITER diagnostic ports, are presented. The outgassing rate of boron carbide ceramics produced by Virial Ltd meets the requirements of the ITER Vacuum Handbook. Massive use of ceramics in ITER may create a significant gas load on the vacuum system that requires accurate analysis. Calculations of gas emission of Equatorial Port #11 were performed and it was demonstrated that a significant amount of ceramics can be used for neutron protection. Experiments on activation of ceramics and stainless steels by fast neutrons were carried out, which showed a rapid reduction of residual radioactivity and absence of hazardous impurities.

1. Introduction

One of the main tasks of ITER diagnostic port-plug is the integration and neutron protection of diagnostics [1,2], as well as reducing the radiation background in the area of reactor elements requiring access for maintenance personnel. The weight restrictions do not allow a significant amount of metal to be used for radiation protection. Due to the low atomic weight and high absorption cross-section of thermal neutrons, boron carbide can serve as an effective flux attenuator for both fast and thermal neutrons. Properties of ceramic based on boron carbide essentially depend on the technology of its manufacture. Boron carbide is thermally stable, chemically inert, has low density (sintered ceramics ~2.33 g/cm^3, hot pressed 2.52 g/cm^3, reaction bonded ~2,64 g/cm^3). Manufacturers have extensive experience in the production of this material but the vacuum properties of ceramics have not been studied in detail before. Ceramics samples were submitted by some Russian manufacturers: Virial, Ltd. (St. Petersburg, http://www.virial.ru), NEVZ-Ceramics (Novosibirsk, http://www.en.nevz.ru) and RCS Energy, Ltd. (Tver', http://www.ekzivent.ru/).

Since the conceptual design stage of ITER diagnostic ports was not supposed to use ceramics, and in the final stage of port design it is planned to use a large number of ceramics, it requires careful confirmation of the possibility of using a large number of ceramics in a ITER

vacuum vessel. I.e., the ceramic should not contain dangerous contaminants, and shall meet the requirements of the ITER Vacuum Handbook (IVH) [3]. Earlier experiments [4–6] were carried out with different types of boron carbide ceramics from different manufacturers, which showed that ceramics do not contain impurities prohibited in ITER, its thermal properties correspond to the literature data. Vacuum properties of small batches of various ceramics have also been investigated in Budker Institute of Nuclear Physic (BINP) [4–6]. The BINP has extensive experience in the study of materials for fusion using various technologies [7], including electron [8–10] and proton [11–13] beams, synchrotron radiation [14,15].

2. Long-term outgassing test of large quantities of sintered ceramics

The outgassing test was conducted to confirm that the ceramic meets the requirements of the IVH [3], i.e. outgassing rate is not more than $1 \cdot 10^{-7}$ Pa $m^3 \cdot s^{-1}$ m^{-2} for hydrogen and not more than $1 \cdot 10^{-9}$ Pa $m^3 \cdot s^{-1}$ m^{-2} for all other impurities. Measurements of the outgassing rate into the vacuum were performed according ITER Vacuum Handbook Appendix 17 [16]. In order to obtain reliable data, tests were carried out with a large number of ceramics. We used 638 samples of 55*55*5 mm in size, with a total area of 4.56 m^2 (Fig. 1). These are the most reliable
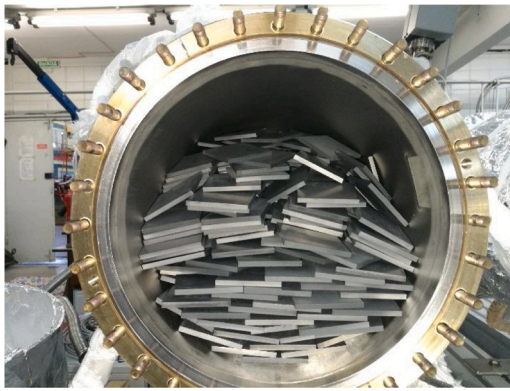

Fig. 1. 638 bars of sintered ceramics inside high vacuum test-bench before measurements. Ceramics produced by Virial. Total surface area of samples is 4.56 m^2.

outgassing tests in the ITER IDM database [17]. For comparison, most other vacuum tests in the IDM database were performed on one or several samples.

To prepare for conducting measurements, the sample was cleaned with ethyl alcohol and in an ultrasonically agitated bath of distilled water, baked at 1000 °C in vacuum prior to testing. Then, from the vacuum furnace, the samples were transferred to a high-vacuum measuring stand.

Vacuum Test Procedure:

1) Ramp up from room temperature to 200 °C: 10 h.
2) Steady temperature at 200 °C for 11 h.
3) Ramp up to 240 °C: 1 h.
4) Steady temperature at 240 °C for 24 h.
5) Cool down to room temperature: 18 h.
6) Ramp up to 100 °C: 3 h.
7) Steady temperature at 100 °C for testing.

After reaching a temperature of 100 °C, measurements were made. Research of dependence of outgassing of sintered ceramics depending on duration of stay in vacuum has been conducted. The samples were not taken out of the vacuum chamber for over a year (pumping has not been turned off) and every 3 months measurements were made (before measurements, samples were heated up to 100 °C, measurements were made at steady temperature at 100 °C (Figs. 2 and 3), then samples cooled down to room temperature, measurements were repeated at room temperature).

After a year in a vacuum, the outgassing rate is strongly reduced: outgassing rate was reduced by three times, to $2.95 \cdot 10^{-9}$ Pa m$^3 \cdot$s^{-1} m^{-2} (Table 1). Sintered ceramic outgassing rate meets IVH [3] requirements with a large reserve.
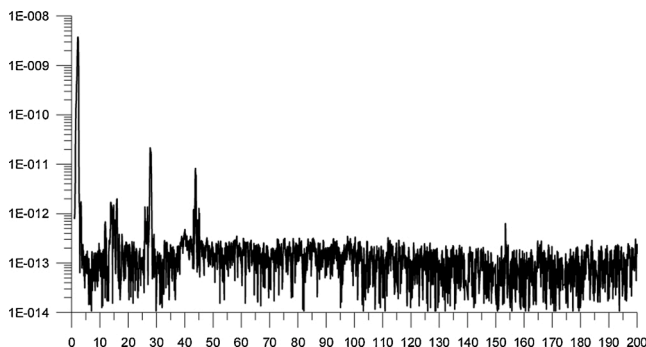

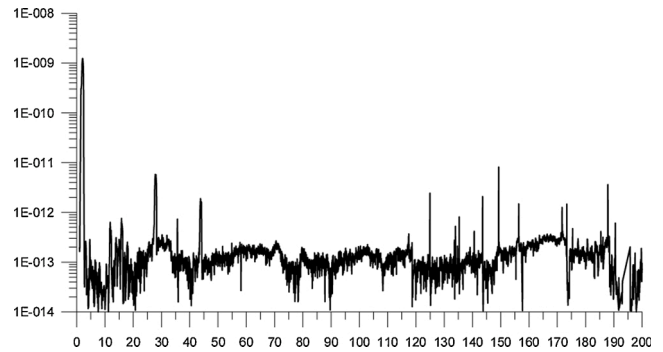**Fig. 2.** RGA (residual gas analyzer) scan for Virial-sintered boron carbide after 24 h at 100 °C.

Fig. 3. RGA scan at 100 °C for the same ceramics after one year in vacuum (at room temperature).

Table 1
Dependence of sintered ceramic outgassing rate at 100 °C on time in vacuum (at room temperature).

Time in vacuum	Outgassing rate [Pa m$^3 \cdot$s^{-1} m^{-2}]
5 h	$10.4 \cdot 10^{-9}$
24 h	$10.0 \cdot 10^{-9}$
29 h	$9.96 \cdot 10^{-9}$
8 month	$3.9 \cdot 10^{-9}$
12 month	$2.95 \cdot 10^{-9}$

3. Outgassing Calculation of ITER Equatorial port #11

The assembled ITER Equatorial Port Plug (EPP) consists of three basic parts (Fig. 4):

- Six modules of the Diagnostic First Walls (DFW) which develops the role of first neutron shielding layer and implements the necessary apertures to the plasma required for the operation of the corresponding diagnostic systems assembled in the Port plug.
- Three Diagnostic Shielding Modules (DSM), which provide the neutron shielding to port aperture in order to minimize the activation and the dose in the Port Cell and Interspace area and ports and house diagnostic and service systems. The typical structure of a modular DSM is presented in Fig. 5 showing metal (coloured) and Boron Carbide (in black, Figs. 6 and 7) surfaces exposed to the primary vacuum.
- The EPP structure as main structural element that holds the rest of components, that forms the connection to the Vacuum Vessel being
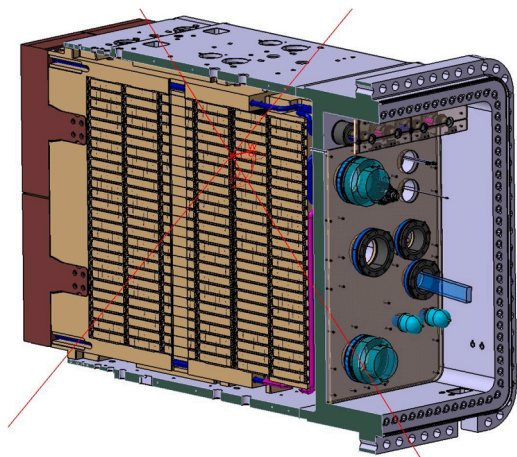

Fig. 4. EP#11 integrated Port Plug. Inside the port plug structure (PPS) there are DSM modules. Port plug section between first and second DSMs is shown.
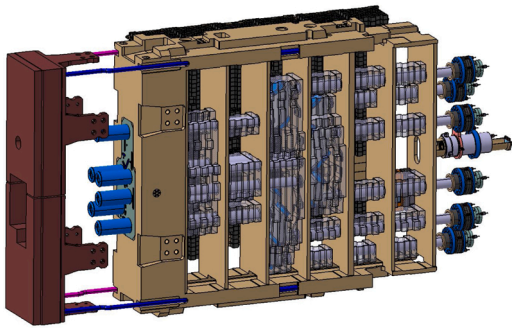
Fig. 5. Typical EP#11 Port Plug DSM Assembly (left – two DFW, center – DSM frame and vertical plates with diagnostics, the back side shows trays with ceramics (Figs. 4 and 5)).
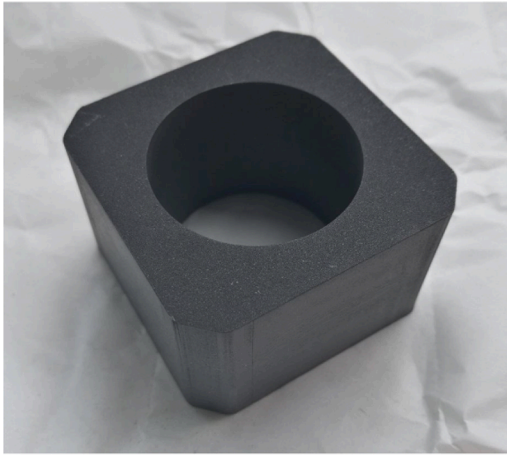

Fig. 6. Sintered B_4C block made by Virial.

Fig. 7. BINP made full scale mockup of shielding tray with hot-pressed blocks made by NEVZ.

part of the primary vacuum and confinement boundaries and that provides the interface (closure plate) for all required penetrations and feedthroughs between the in-vessel space and the Port Cell.

In Ref [18] the acceptable gas load from the equatorial port ($1.42 \cdot 10^{-5}$ Pa $m^3 \cdot s^{-1}$) is calculated based on Chapter 17.8.1 of Ref [16]. In Ref [18] estimates of the exposed area of elements in vacuum and total gas emission of the Equatorial port #12 were made. By analogy with [18] we will calculate areas of elements in vacuum (Table 2) and full gas emission of EP11 (Tables 3 and 4).

The estimated number of B_4C blocks is the three DSMs (DSM#1 12606 blocks, DSM#2 11930 blocks, DSM#3 15278 blocks) of EP#11 is $39814 \approx 40000$ blocks. B_4C blocks are arranged on shielding trays as

Table 2
Summary of total vacuum exposed surface for SS components of EP#11.

Component	Area [m^2]
Vertical plates	33.6
DSM Frame	36.2
Backfilling	40.4
Shielding Trays	157.4
PPS-DSM interfaces	32.4
DFWs	13.5
Port Plug Structures	61.3
Total	374.8

Table 3
Gas load at 100 °C at the EPP#11.

Material	Area [m^2]	Outgassing rate [Pa m^3 s^{-1} m^{-2}]	Outgassing load [Pa m^3 s^{-1}]
B_4C ceramics	407	$1 \cdot 10^{-8}$	$4.07 \cdot 10^{-6}$
Stainless steel	375	10^{-8}	$3.75 \cdot 10^{-6}$
Total	782		$0.78 \cdot 10^{-5}$

Table 4
Gas load at 100 °C at the EPP#11 for cases where ceramics have been in a vacuum for over a year.

Material	Area [m^2]	Outgassing rate [Pa $m^3 \cdot s^{-1}$ m^{-2}]	Outgassing load [Pa $m^3 \cdot s^{-1}$]
B_4C ceramics	407	$2,95 \cdot 10^{-9}$	$1.20 \cdot 10^{-6}$
Stainless steel	375	10^{-8}	$3.75 \cdot 10^{-6}$
Total	782		$0.495 \cdot 10^{-5}$

shown in Fig. 7. Vacuum exposed surface of a single block (size 46*46*28 mm with a center hole 30.5 mm in diameter, Fig. 6) is 0.0102 m^2. Therefore, the total B_4C exposed surface for EP#11 will be 407,1 m^2. Estimates of the area of individual steel elements and the total area of steel in EP#11 are shown in Table 2.

Separately, it should be noted that in Ref [18] the steel outgassing rate is incorrectly estimated ($10^{-9} \div 10^{-10}$ Pa $m^3 \cdot s^{-1}$ m^{-2}). It is taken from Section 17.9.3 Ref [16], which provides data for room temperature, not for 100 °C. We use stainless steel outgassing rate assessment for 100 °C (10^{-8} Pa m^3 s^{-1} m^{-2}) based on average values from vacuum tests, including background outgassing of steel walls of high vacuum test benches [4–6,17,19].

It is to be noted that the calculated value remains below the maximum outgassing estimated for a single Equatorial Port Plug ($1.42 \cdot 10^{-5}$ Pa m^3 s^{-1} [18,19]).

In November 2020, the ITER Director General approved a Reviewer report [20] that limited the port outgassing to $5 \cdot 10^{-5}$ Pa $\cdot m^3 \cdot s^{-1}$, and recommended that the ceramic outgassing rate be limited to $1 \cdot 10^{-8}$ Pa $m^3 \cdot s^{-1}$ m^{-2}. Measurements of ceramic outgassing and calculations of port outgassing show that EPP#11 satisfies these requirements. Thus, the use of large quantities of boron carbide ceramics in vacuum to protect ITER diagnostic ports is acceptable.

4. Activation of B_4C ceramics and SS 316L-ITER Grade by fast neutrons

At the BINP for the development of boron neutron capture therapy of malignant tumors [21], an accelerator source of epithermal neutrons was proposed and created [11]. The source consists of an electrostatic vacuum-insulated tandem accelerator for obtaining a stationary proton beam with an energy of 2.3 MeV and a current of 10 mA, a lithium target

for generating neutrons as a result of the ^{7}Li(p,n)^{7}Be threshold reaction, and a formation system for obtaining a therapeutic beam of epithermal neutrons.

In the accelerator, a 2.1 MeV 1,4 mA deuteron beam is also obtained, and fast neutrons are generated on a lithium target with a yield of $2 \cdot 10^{12}$ second^{-1} [22]. The Li(d,n) reaction proceeds in two ways: ^{7}Li(d,n)^{8}Be and ^{7}Li(d,n)2^{4}He. The neutron spectrum contains two components: with an average energy of 13 MeV, due to the first pathway of neutron generation, and 3 MeV, due to the second pathway. The average neutron energy is 5.68 MeV [23]. Two samples of hot pressed boron carbide from NEVZ with a size of 46*46*29 mm with a hole in the middle were irradiated with a flux of fast neutrons for 20 min. And sintered B$_4$C from Virial, tiles 55*55*5 mm and a sample of stainless steel 316L-ITER Grade (IG) with a size of 130*130*40 mm, placed at a distance of 10 cm from the target. The flux density was $3 \cdot 10^9$ neutrons/cm$^2 \cdot$s for 20 min and the cumulated fluence was $3.6 \cdot 10^{12}$ neutrons/cm^2. Which roughly corresponds to the conditions inside the DSM, where the characteristic neutron fluxes are $10^8 \div 10^{11}$ n/cm$^2 \cdot$s [24]. Inside the ITER port-plug, neutrons have a wide energy spectrum, with energies of $0.1 \div 1$ MeV dominated; the spectrum is given in the Ref. [24].

The activation of the samples was measured with a DKS-96 dosimeter (OOO Doza, Russia) applied close to the samples. The dose rate of boron carbide samples was 50 μSv/h after the end of irradiation and 0.14 μSv/h (natural background level) after 3 days. The dose rate of the steel sample was 1500 μSv/h after the end of irradiation and 1.77 μSv/h after 3 days.

The level of induced radiation from activated steel 316 L(N)-ITER Grade decreases faster (by a thousand times in 3 days), because first the main activity is due to decay of ^{56}Mn with a half-life of 2.58 h. The radioactivity of ceramics declines more slowly - a 300-fold decrease after 3 days.

ITER requirements for impurities in materials [25]: Co – max 0.05 % by weight, Ta - max 0.01 %, Nb – max 0.01 %. Impurities content by weight in ceramics previously was measured by using scanning electron microscope equipped with energy-dispersive X-ray spectroscopy [4]. Hot pressed boron carbide from NEVZ: B$_4$C 99.8 %, O $0-0.1$%, Si $\sim$0.2 %, Al less 0.01 % by weight. Sintered B$_4$C from Virial: B$_4$C 99 %, O less 1%, Si less 0.2 %, Al less 0.04 % [4].

The results of experiments on activation of ceramics and stainless steel 316L-IG by low-energy neutrons are presented in Ref [5]. The manganese content in these two types of ceramics was estimated at 0.0001 % [5].

The spectrum of the induced activity of the samples was measured with a SEG-1KP-IFTP gamma-ray spectrometer based on a semiconductor detector made of highly pure germanium. In Fig. 8 shows the spectrum of two samples of boron carbide ceramics, Virial and NEVZ, placed close to the detector. Spectrum measurements for 3 min were started 32 and 42 min, respectively, after the end of neutron generation. The spectrum contains lines of 511 keV (^{22}Na), 843 keV (^{27}Mg), 846 keV (^{56}Mn), 1276 keV (^{22}Na), 1368 keV (^{24}Na). These isotopes were produced by fast neutrons from aluminum in reactions ^{27}Al (n,α) ^{24}Na, ^{27}Al (n,spall) ^{22}Na, ^{27}Al (n,p) ^{27}Mg and from manganese in reaction ^{55}Mn (n,γ)^{56}Mn. The manganese content in the two types of ceramics is the same, so the 846 keV (^{56}Mn) peak has the same height. The aluminum content is different, so the other peaks in hot-pressed ceramics are lower.

In Fig. 9 shows two spectra of a steel 316L-IG sample measured for 1 min after 28 min (the sample is placed at a distance of 50 cm from the detector) and after 3 days 2 h 42 min (the sample is placed close to the detector) after the end of neutron generation. Immediately after the end of neutron generation, the main dose rate is due to the decay of the atomic nucleus ^{56}Mn, after 3 days - atomic nuclei ^{58}Co (811 keV), ^{54}Mn and ^{99}Mo. The first isotope appeared in reaction ^{58}Ni(n,p)^{58}Co (steel contains 12 % Ni). Manganese-56 could appear in reactions ^{56}Fe(n,p)^{56}Mn and ^{55}Mn(n,γ)^{56}Mn (steel contains 1.85 % Mn). 2.4 % of molybdenum in steel gives reactions ^{98}Mo(n,γ)^{99}Mo and ^{100}Mo(n,2n)^{99}Mo.

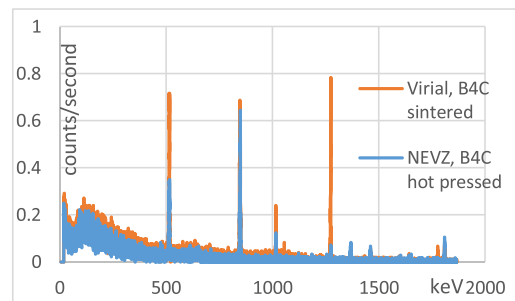Studies have shown that boron carbide ceramics meet all ITER

Fig. 8. Gamma-ray spectrum of two samples of boron carbide ceramics after activation of fast neutrons.
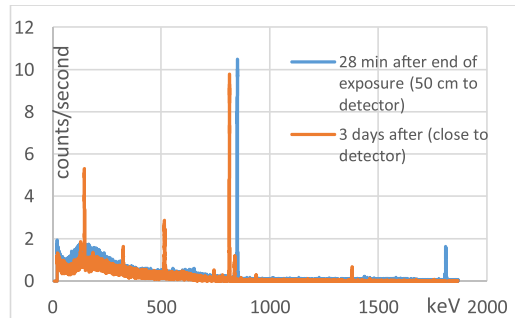

Fig. 9. Gamma-ray spectrum of SS 316L-IG after 28 min after the end of neutron generation (the sample is placed at a distance of 50 cm from the detector) and after 3 days (the sample is placed close to the detector).

requirements in terms of chemical composition, vacuum and thermal properties. The BINP together with the Russian domestic agency ITER (RF-DA) prepared and agreed with the ITER Organization the technical specification for B$_4$C ceramics [26], on the basis of which the procurement of ceramics for the ITER diagnostic ports can begin. The BINP is the manufacturer and integrator of EP#11 [1] and has already started preparing a contract with the ceramic supplier.

Boron carbide provides good neutron protection due to the main (n,α) reaction: ^{10}B + n → ^{4}He + ^{7}Li + γ (93.9 %) +2.79 MeV. With fast neutrons (E > 1.2 MeV) there is a secondary reaction ^{10}B + n → 2 ^{4}He + T. Though this reaction has a very less probability compared to n,α reaction, it has great importance from the viewpoint of reactor waste. The ITER organization conducted calculations of the residual radioactivity of EPP-11 elements [27]. The specific activity of B$_4$C ceramics is calculated to be $1.65 \cdot 10^9$ Bq/g. Taking into account the weight of the ceramics in the DSM ($\sim$1.2 tons), its contribution is no more than 20 % of the DSM activity (total weight 10 tons). For example, a steel DSM frame weighing 4.5 tons would have a similar specific activity of $2 \cdot 10^9$ Bq/g [27].

Declaration of Competing Interest

The authors declare that they have no known competing financial interests or personal relationships that could have appeared to influence the work reported in this paper.

Acknowledgments

References

[1] Yu.S. Sulyaev, E.V. Alexandrov, A.V. Burdakov, et al., Engineering calculations and preparation for manufacturing of ITER equatorial port #11, IEEE Trans. Plasma Sci. 48 (6) (2020) 1631–1636, https://doi.org/10.1109/TPS.2020.2985113.

[2] A. Listopad, E. Alexandrov, A. Burdakov, et al., Preliminary design of the ITER upper ports #02 and #08 integration, IEEE Trans. Plasma Sci. 48 (6) (2020) 1721–1725, https://doi.org/10.1109/TPS.2020.2985401.

[3] ITER Vacuum Handbook, 2019. Reference: ITR-19-004, https://www.iter.org/technical-reports.

[4] A. Shoshin, A. Burdakov, M. Ivantsivskiy, et al., Properties of boron carbide ceramics made by various methods for use in ITER, Fusion Eng. Des. 146B (2019) 2007–2010, https://doi.org/10.1016/j.fusengdes.2019.03.088.

[5] A. Shoshin, A. Burdakov, M. Ivantsivskiy, et al., Qualification of boron carbide ceramics for use in ITER ports, IEEE Trans. Plasma Sci. 48 (6) (2020) 1474–1478, https://doi.org/10.1109/TPS.2019.2937605.

[6] 55. QB- R&D report on Boron Carbide Ceramics, ITER_D_X7RY7E, 2018.

[7] A.A. Shoshin, et al., Study of plasma-surface interaction at the GOL-3 facility, Fusion Eng. Des. 114 (2017) 157–179, https://doi.org/10.1016/j.fusengdes.2016.12.019.

[8] A.A. Vasilyev, et al., In-situ imaging of tungsten surface modification under ITER-like transient heat loads, Nucl. Mater. Energy 12 (2017) 553–558, https://doi.org/10.1016/j.nme.2016.11.017.

[9] L.N. Vyacheslavov, et al., Diagnostics of the dynamics of material damage by thermal shocks with the intensity possible in the ITER divertor, Phys. Scr. 93 (2018), 035602, https://doi.org/10.1088/1402-4896/aaa119.

[10] L. Vyacheslavov, et al., In sity study of the processes of damage to the tungsten surface under transient heat loads possible in ITER, J. Nucl. Mater. 544 (2021), 152669, https://doi.org/10.1016/j.jnucmat.2020.152669.

[11] S. Taskaev, Accelerator based epithermal neutron source, Phys. Part. Nuclei 46 (6) (2015) 956–990, https://doi.org/10.1134/S1063779615060064.

[12] D. Kasatov, A. Makarov, I. Shchudlo, S. Taskaev, A study of gamma-ray and neutron radiation in the interaction of a 2 MeV proton beam with various materials, Appl. Radiat. Isot. 106 (2015) 38–40, https://doi.org/10.1016/j.apradiso.2015.08.011.

[13] A. Badrutdinov, et al., In Situ observations of blistering of a metal irradiated with 2-MeV protons, Metals 7 (12) (2017) 559, https://doi.org/10.3390/met7120558.

[14] A.S. Arakcheev, et al., Applications of synchrotron radiation scattering to studies of plasma facing components at Siberian synchrotron and terahertz radiation centre, in: AIP Conf. Proc, 1771, 2016, https://doi.org/10.1063/1.4964211, 060003.

[15] A.S. Arakcheev, et al., Dynamic observation of X-ray Laue diffraction on single-crystal tungsten during pulsed heat load, J. Synchrotron Rad. 26 (2019) 5, https://doi.org/10.1107/S1600577519007306.

[16] ITER Vacuum Handbook Appendix 17 Guide to Outgassing Rates and their Measurement, ITER_D_2EXDST, 2009.

[17] Outgassing test report sintering boron carbide made by Virial, ITER_D_X7RXSC, 2021.

[18] Report Outgassing Calculation of equatorial 12 (55.QC), ITER_D_45WED8, 2020.

[19] 55. QB Outgassing Calculation, ITER_D_4QY98M, 2021.

[20] DPI-PT Mini Review of B4C Outgassing – Independent Reviewer Report, ITER_D_47TDJ4, 2020.

[21] W. Sauerwein, A. Wittig, R. Moss, Y. Nakagawa (Eds.), Neutron Capture Therapy: Principles and Applications, Springer, 2012, https://doi.org/10.1007/978-3-642-31334-9.

[22] D. Kasatov, A. Koshkarev, A. Makarov, et al., Fast-neutron source based on a vacuum-insulated tandem accelerator and a lithium target, Instrum. Exp. Techn. 63 (5) (2020) 611–615, https://doi.org/10.31857/S0032816220050158.

[23] K. Mitrofanov, V. Piksaikin, K. Zolotarev, et al., The energy spectrum of neutrons from 7Li(d,n)8Be reaction at deuteron energy 2.9 MeV, in: EPJ Web of Conf, 146, 2017, p. 11041, https://doi.org/10.1051/epjconf/201714611041.

[24] N. Casal, et al., Functional materials for ITER diagnostic systems – radiation aspects, Fusion Eng. Des. 125 (2017) 277–282, https://doi.org/10.1016/j.fusengdes.2017.08.017.

[25] Chemical composition and impurity requirements for materials, ITER_D_REYV5V, 2016.

[26] 55. QB Material Specification for the supply of Boron Carbide (B4C), ITER_D_457TBH, 2021.

[27] 55. QB - Checklist for Radwaste Inventories, ITER_D_SL86JE, 2021.